Journal of Luminescence 205 (2019) 324–328

Contents lists available at ScienceDirect

Journal of Luminescence

journal homepage: www.elsevier.com/locate/jlumin

TL in green tourmaline: Study of the centers responsible for the TL emission by EPR analysis

Nilo F. Cano[a,*], T.K. Gundu Rao[b], Jorge S. Ayala-Arenas[c,*], Carlos D. Gonzales-Lorenzo[b], Letícia M. Oliveira[d], Shigueo Watanabe[b,*]

[a] Instituto do Mar, Universidade Federal de São Paulo, Rua Doutor Carvalho de Mendonça, 144, CEP 11070-100 Santos, SP, Brazil
[b] Instituto de Física, Universidade de São Paulo, Rua do Matão, Travessa R, 187, CEP 05508-090 São Paulo, SP, Brazil
[c] Escuela Profesional de Física, Facultad de Ciencias Naturales y Formales, Universidad Nacional de San Agustín (UNSA), Av. Independencia S/N, Arequipa, Peru
[d] Instituto de Pesquisas Energéticas e Nucleares, IPEN-CNEN/SP, Av. Prof. Lineu Prestes, 2242, Cidade Universitária, 05508-000 São Paulo, SP, Brazil

ARTICLE INFO

Keywords:
TL
EPR
Radiation dosimetry
Silicate
Tourmaline

ABSTRACT

Electron paramagnetic resonance (EPR) studies have been carried out to identify the defect centers responsible for the thermoluminescence (TL) peaks in the mineral tourmaline. The mineral exhibits three TL peaks approximately at 170, 250 and 310 °C. The EPR spectrum of the green tourmaline sample pre-heated to 500 °C presented a large signal around $g = 4.3$ due to Fe^{3+} ion. Room temperature EPR spectrum of irradiated green tourmaline shows the formation of two defect centers in the region of $g = 2.0$. One of the centers (center II) with a g factor equal to 1.96 is identified as an F^+-center and is related to the observed high temperature 250 and 310 °C TL peaks. Center I exhibiting a doublet is due to hydrogen atoms (H^0), stable in the crystal lattice at room temperature and this center correlates with the TL peak at 170 °C of the green tourmaline. An optical absorption measurement also was carried out. Bands at around 430, 730 and 1100 nm have been observed.

1. Introduction

The silicate minerals are, in general, excellent thermoluminescent materials, some of them with high sensitivity to low as well as high radiation doses [1–7]. Hence, they are candidates for radiation dosimetry.

There is one group of silicates called ring silicates or cyclosilicate to which belong beryl, cordierite and tourmaline. The tourmaline structure is typically rhombohedral with space-group *R*3*m* [8–10], although some studies report lower symmetry such as orthorhombic, monoclinic or triclinic [11–13]. The structure is characterized by groups of XO_9, YO_6, TO_4, and BO_3 polyhedra connected to each other through ZO_6 octahedra. The latter are arranged in a 3-D framework and are linked to the YO_6 octahedron through the O3–O6 edge. The tourmaline has a complex formula, $XY_3Z_6(T_6O_{18})(BO_3)_3V_3W$, where X, Y and Z sites can be occupied by different ions [8–10]. Therefore, about 12 varieties of tourmaline are formed in nature. According to several authors [14–17], the following ions fit into the following structural sites: X = Na, Ca, o (= vacancy), K; Y = Al, Fe^{3+}, Cr^{3+}, V^{3+}, Mg, Fe^{2+}, Mn^{2+}, Cu^{2+}, Zn, Li, Ti^{4+}, o; Z = Al, Fe^{3+}, Cr^{3+}, V^{3+}, Mg, Fe^{2+}; T = Si, Al, B, Be; B = B, (o); W(O1) = OH, F, O; V(O3) = OH, O.

Tourmaline is a well known silicate mineral because some of its varieties have high gemological value [18,19].

The tourmaline crystal has been widely investigated by many authors through spectroscopic methods such as Mössbauer spectroscopy, UV–Vis spectroscopy, Raman spectroscopy and other spectroscopic techniques due to its color and gemological value [20–36].

Several authors [37–42] measured the effects of thermal treatments and irradiation on optical absorption spectra of natural tourmaline of different color and discussed the crystal field effect on the energy levels of transition ions, mostly Mn^{2+}, Mn^{3+}, Fe^{2+}, Fe^{3+} and Ti^{4+}, usually responsible for the coloration of the crystal. In contrast, studies on luminescence properties and the identification of the defects responsible for emission of the TL peaks of the tourmalines crystal so far are few.

The process of irradiation and thermal treatment can change some physics properties of the mineral that are dependent on point defects, such as luminescence and electron paramagnetic resonance. These properties make tourmaline crystal an interesting material for some applications like dosimetry. However, although it has been a subject of some experimental studies, an investigation of defect centers created by ionizing radiation responsible for TL properties of tourmaline is still lacking. The identification and characterization of these centers form an essential step in understanding the mechanisms of TL emission. In this context, EPR provides a convenient and sensitive technique for such a

* Corresponding authors.
E-mail addresses: nilocano@if.usp.br, nilo.cano@unifesp.br (N.F. Cano), jayala@unsa.edu.pe (J.S. Ayala-Arenas), watanabe@if.usp.br (S. Watanabe).

https://doi.org/10.1016/j.jlumin.2018.09.034
Received 2 May 2018; Received in revised form 13 September 2018; Accepted 15 September 2018
Available online 15 September 2018

study, as it helps in providing support and further identification of the paramagnetic species by EPR technique.

In the present work a green tourmaline sample was studied using the TL and EPR techniques to investigate the centers responsible for their TL properties and possible applications in gamma radiation dosimetry. No published papers in the literature were found related to study here carried out. Optical absorption measurements also have been carried out.

2. Material and experimental

A natural green tourmaline crystal from Teofilo Otoni, state of Minas Gerais, Brazil, was investigated in this work. The sample was crushed and sieved retaining grains with 0.080–0.180 mm diameters for TL and EPR analysis. Powder with diameter smaller than 0.080 mm were used for an analysis by X-ray Fluorescence (XRF) and X-ray diffraction (XRD) in order to determine the composition and to perform the structural analysis of the samples acquired as tourmaline.

XRF analysis was carried out in the Laboratory of Technological Characterization from the Polytechnic School of the University of São Paulo. The values presented were determined in a sample fused with anhydrous lithium tetraborate in the calibration ROC-1 (Rocks), relative to the quantitative analysis comparing them with certified reference materials in an XRF spectrometer, PANalytical, Zetium model. The major oxides are expressed as percentage by weight (wt%) and the estimated error is < 5%.

The crystalline phases of the green tourmaline was investigated by XRD using the MiniFlex 300 from Rigaku, with Cu Kα radiation (λ = 1.5418 Å), and the data collected by scanning 2θ from 10° to 90° at room temperature.

Sieved samples as described above were each divided into several portions to be irradiated to several γ-ray doses.

For irradiation, Institute for Energy and Nuclear Researches Radiation Center's ^{60}Co source was used for γ-doses below 1 kGy.

The TL measurements were carried out in a Harshaw TL Reader, model 4500, equipped with a bialkali photomultiplier (PMT) for light detection. The applied heating rate was 4 °C/s in nitrogen atmosphere.

A Miniscope EPR spectrometer operating at X-band frequency with 100 kHz modulation frequency was utilized for the EPR experiments. Diphenyl Picryl Hydrazyl (DPPH) was used for calibrating the g-values of the defect centers.

For optical absorption measurement, the green tourmaline sample was sliced with approximately 2.0 mm of thickness. Then it was polished on both faces. The optical spectrum was obtained using the Cary 500 spectrophotometer from 350 to 2000 nm range.

3. Results and discussions

Table 1 shows the composition in weight % of the oxide components of the tourmaline samples using the XRF analysis; several oxide components were not listed (with less than 0.01%) in the table and some oxide components were not detected due to limitations of the XRF technique. This analysis was performed to identify which are the chemical elements in the samples, and for future studies about which of these elements are responsible for the TL and EPR signals. Besides basic oxide components SiO_2 and Al_2O_3, oxides such as Na_2O, Fe_2O_3, K_2O, ZnO, CaO, Na_2O and others in smaller concentration are found.

There are many types of tourmaline [8], but from XRF analysis shown in Table 1 it seems that the sample here discussed can be Schorl.

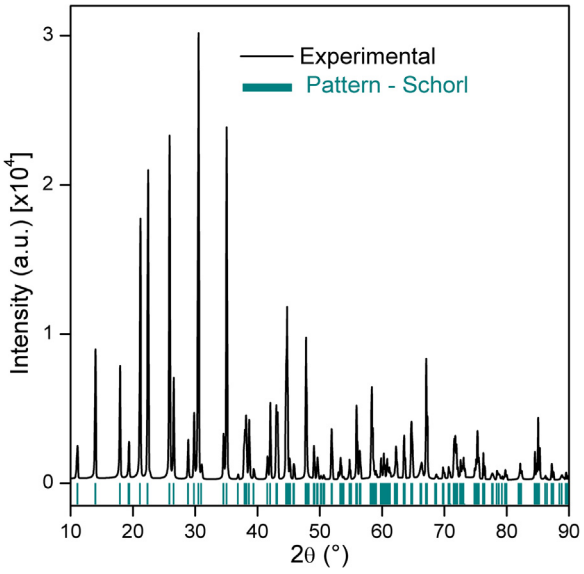

Fig. 1. X-ray diffraction of the green tourmaline crystal compared with XRD pattern from JCPDS card, No. 43-1464 (Schorl).

The high content of Fe_2O_3 is a main indication. We assume that the structure of our tourmaline sample is similar to that of magnesium tourmaline. In the place of Mg we have Fe^{2+} [43].

The diffractogram of the green tourmaline natural sample is shown in Fig. 1. Comparing the powder XRD pattern to the JCPDS files, all the peaks of the crystal are identified as belonging to tourmaline variety with present of Fe denominate Schorl ($NaFe_3^{2+}Al_6Si_6O_{18}(BO_3)_3(OH)_4$) (JCPDS card, No. 43-1464). This result confirms the identification of the tourmaline variety by chemical XRF analysis.

TL glow curves of green tourmaline samples heat-treated at 500 °C for 30 min and irradiated with γ-doses from 10 to 1000 Gy show three peaks at 170, 250 and 310 °C as can be seen in Fig. 2.

Fig. 3 shows the TL response of the three peaks as a function of ^{60}Co γ-ray radiation doses between 10 and 1000 Gy. Analyzing the dose response curves with log axes in the same scale, as shown in Fig. 3, it can be observed that the TL response of peaks at 250 and 310 has a linear behavior as the curve slope equals to 45° in the dose range of 10 Gy to 1 kGy. Whereas peak at 170 °C is supra-linear for doses between 10 and 100 Gy and then is linear. For low doses less than 10 Gy the sample is not very sensitive. This result shows that the peaks at 250 and 310 °C can be used in dosimetry for dose above of 10 Gy.

The emission curve of the green tourmaline sample was analyzed by the Glow Curve Deconvolution Function (GCDF) method to determine kinetic TL parameters using a second order (symmetrical) equation from Kitis et al. [44]. Mathcad software was used to create the deconvolution program. The program is based on chi-square minimization. Quality of fit was tested with the Figure of Merit (FOM) [45]. The TL parameter results determined by GCDF method are shown in Table 2. FOM = 1.25% shows that data fit is satisfactory. Fig. 4 shows the three TL peaks separated using second-order kinetics in the region between 50 and 400 °C.

Prior to gamma irradiation, tourmaline EPR spectrum at room temperature exhibits a low field line at about 1580 G (Fig. 5). The measured *g*-value of this line is 4.28 and the line arises from Fe^{3+} ion which is present in tourmaline as an impurity. The intensity of this

Table 1
Oxides composition in green tourmaline samples using X-ray fluorescence analysis.

Compound	SiO_2	Al_2O_3	Na_2O	Fe_2O_3	K_2O	ZnO	CaO	MnO	TiO_2	PbO
(wt%)	52.1	37.7	2.12	2.06	0.43	0.26	0.24	0.13	0.11	0.02

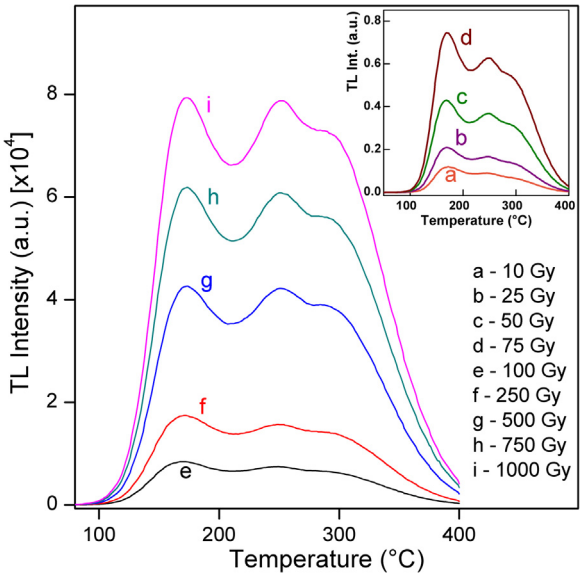

Fig. 2. TL glow curves of green tourmaline crystals pre-annealed at 500 °C for 30 min and irradiated at several γ doses.

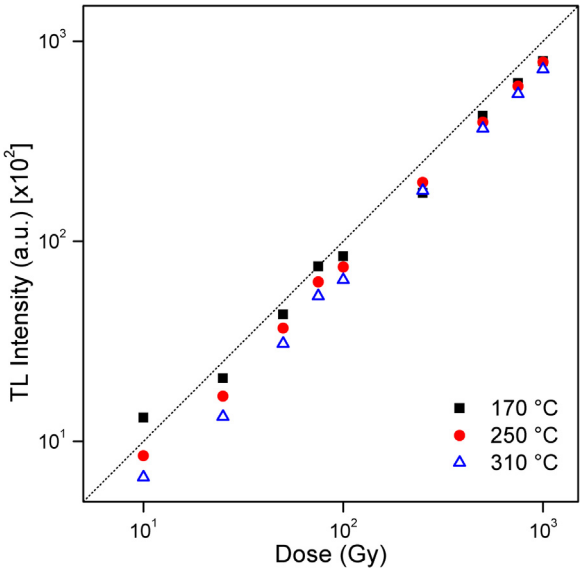

Fig. 3. TL intensity behavior of the TL peaks at 170 °C, 250 °C and 310 °C as a function of gamma radiation doses, the dashed line indicates linearity.

Table 2
TL parameters of the green tourmaline sample taken by GCDF. FOM = 1.25%.

Peak	Kinetic order	Tm (°C)	Activation energy (eV)
1	2st	173.4	0.80
2	2st	249.5	1.0
3	2st	312.0	1.3

signal does not change with gamma irradiation. On gamma irradiation, the EPR spectrum recorded at room temperature is shown in Fig. 5. A single EPR line is seen near the free-electron region as well as a clear doublet separated by 513 G. Thermal annealing experiments indicate that the observed spectrum has contributions from two defect centers. These two centers are labelled in Fig. 5. The measured *g*-value of center I is 2.0146. The doublet spectrum closely resembles the doublet spectrum observed in gamma irradiated calcium phosphate [46,47] and acidic glasses [48,49].

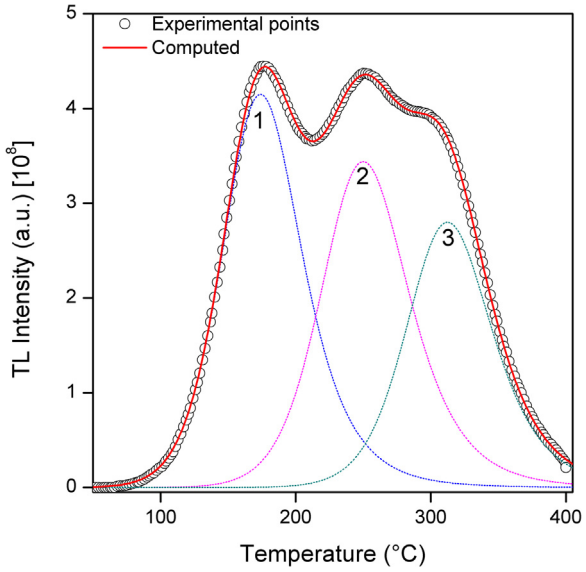

Fig. 4. TL glow curve from green tourmaline pre-annealed at 500 °C for 30 min and subsequently receiving a γ-ray dose of 1 kGy. A good fit between the experimental glow curve (open circles) and the simulated glow curve (full line at red) can be achieved by assuming the presence of three peaks.

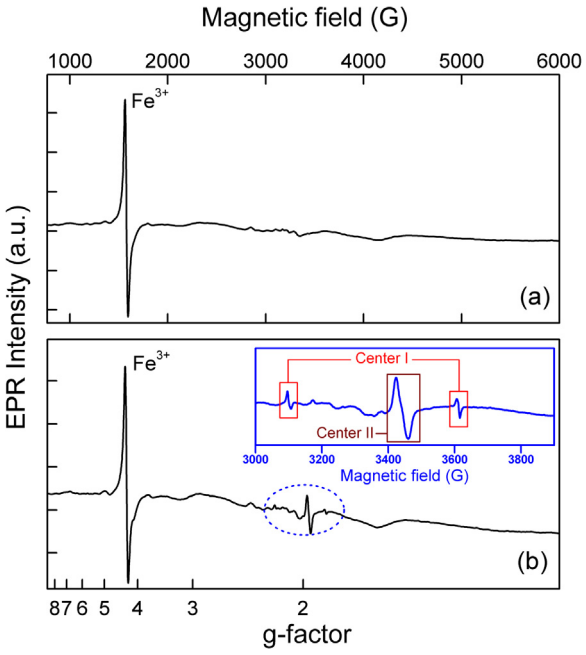

Fig. 5. Room temperature EPR spectra of green tourmaline: (a) as-received, (b) Irradiated sample (Dose: 1 kGy) showing a EPR signal at $g = 4.28$ due to Fe^{3+}. The inset in (b), shows center I (H^0-center) and center II (F^+-center).

The separation of the doublet, for example, is 503 G in irradiated Bayerite [50,51]. The doublet spectrum has been assigned to hydrogen atom radicals and arises from the hyperfine coupling of the electron spin of H to the nuclear magnetic moment of hydrogen nuclei. A relatively recent observation of H atoms in a mineral system is in beryl [52].

Based on these observations, center I in tourmaline is assigned to H atom. The EPR spectra obtained after a thermal treatment at 500 °C for 30 min followed by irradiation with different gamma doses are shown in Fig. 6. The thermal annealing results of center I is shown in Fig. 7. The EPR line intensity was determined by measuring the peak-to-peak height of the EPR lines. It is observed that the center becomes unstable

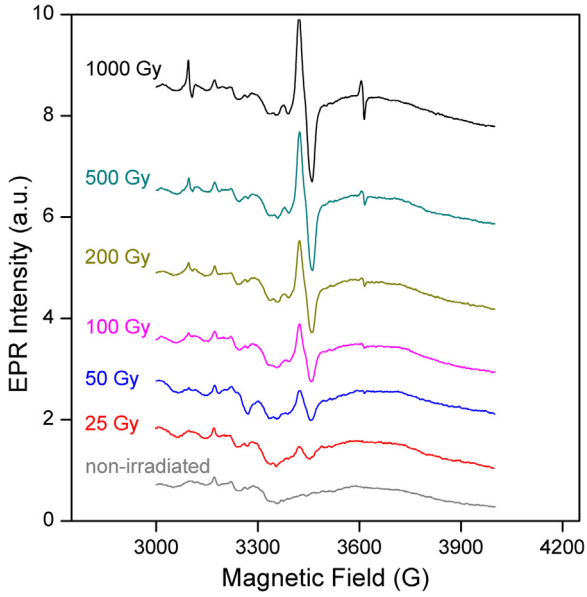

Fig. 6. EPR spectra of green tourmaline pre-annealed at 500 °C for 30 min in air and then irradiated with different gamma doses between 25 Gy and 1000 Gy.

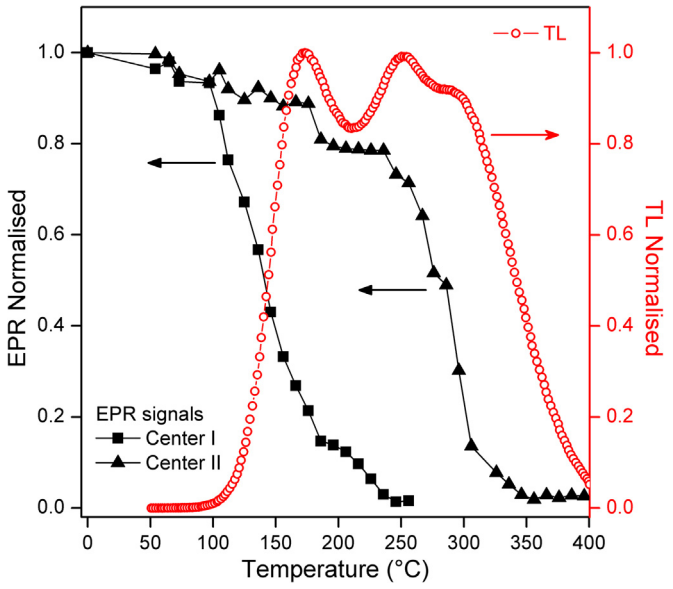

Fig. 7. Decay of the EPR signals center I (filled square) and center II (filled triangle) of the samples submitted to different thermal treatments. TL glow curve from green tourmaline pre-annealed at 500 °C for 30 min and subsequently receiving a γ-ray dose (open circles).

around 100 °C and its intensity is found to decrease in the temperature range extending from 100 °C to 220 °C. This decrease in EPR intensity relates with the TL peak at 170 °C.

Divalent ions like Ca^{2+}, Mg^{2+} and Zn^{2+} are present in the lattice of tourmaline. Tourmaline also contains trivalent (Al^{3+}) and tetravalent (Si^{4+}) ions. A partial substitution of trivalent and tetravalent ions by divalent ions is possible due to anti-site cation exchange. These exchanges are point defects in crystals and are called as cation exchange disorder. Due to cation exchange, oxygen vacancies will be present in tourmaline. Center II shown in Fig. 5 is characterized by an isotropic *g*-value equal to 1.9976 and a linewidth of 36 G. On gamma irradiation, electrons can get trapped at oxygen vacancies to form F^+-centers (an electron trapped at an anion vacancy). F^+-centers have *g*-values close to free-electron value ($g \sim 2.0$) with a *g*-shift which may be negative or

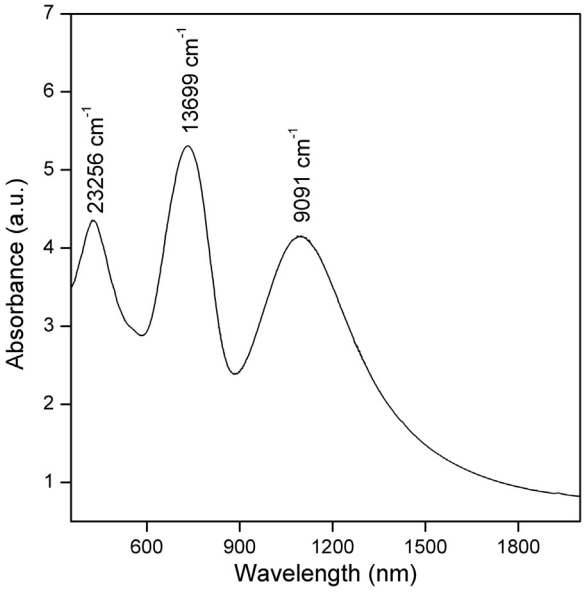

Fig. 8. Optical absorption spectrum of green tourmaline sample.

positive. Linewidth of F^+-centers are decided by the amount of delocalization of the unpaired electron and also on the relative abundance and magnetic moments of the ions present in the lattice. In alkali halides large linewidths are observed as the electron is considerably delocalized. In systems like MgO and CaO, smaller linewidths are observed. Center II in tourmaline has a relatively large linewidth of 36 G and the *g*-value is close to the free-electron value. On the basis of these observations, center II is tentatively ascribed to an F^+-center. It is observed in thermal annealing experiments that center II becomes unstable around 200 °C and decays in the temperature range 200–350 °C. Therefore, it is possible that center II may relate with the TL peak at 250 °C as well as the peak at 310 °C.

Fig. 8 shows optical absorption spectra of green tourmaline slab. Strong bands at 430, 730 and 1100 nm are observed in the sample. According to Deer et al. [8], in tourmaline, containing about 3.5% Fe, the principal colors come from Fe^{2+} *d-d* bands in the 700 nm region; they are usually blue or green. Burns [53] attributes to Fe^{3+} *d-d* transitions $^6A_{1g} \rightarrow {}^4T_{1g}$ producing ν_1-band, $^6A_{1g} \rightarrow {}^4T_{2g}$ ν_2-band and $^6A_{1g} \rightarrow {}^4A_{1g}$, ^4E_g ν_3-band in green tourmaline. ν_1-, ν_2- and ν_3-bands occur at 430 nm (23,256 cm^{-1}), 730 nm (13,699 cm^{-1}) and 1100 nm (9091 cm^{-1}), respectively. Since ν_1-band is blue-violet absorption and ν_2-band is yellow-red absorption the crystal appears to be green colored.

4. Conclusions

The XRD and XRF analysis have shown that sample here investigated have the tourmaline crystal structure with the basic composition of the main oxides corresponding to the tourmaline crystal.

The TL glow curve of the samples heat-treated at 500 °C for 30 min and irradiated with different γ doses present three peaks at 170, 250 and 310 °C. The glow-curve deconvolution shows that in the region from 50 to 400 °C, three overlapped TL peaks of kinetic second order are observed. The TL intensity as function of dose of 250 and 310 °C peaks have shown that its TL intensity grows linearly in the region between 10 and 1000 Gy. As a consequence of the present results, these two TL peaks may be used for radiation dosimetry.

A EPR signal characterized by a single isotropic line at about $g = 4.28$ with large intensity due to Fe^{3+} ion is observed in the EPR spectrum of green tourmaline. This signal is not affected by γ-radiation. Furthermore, two defect centers are identified in the irradiated green tourmaline. Center I exhibiting a doublet signal at $g = 2.0146$ with A

= 513 G is attributed to the hydrogen atoms (H^0-center). Another signal at $g = 1.9976$ is tentatively assigned to F^+-center (center II).

Data correlation analysis of EPR and TL results showed that the center I and the TL peak at 170 °C can be attributed to the same defect. In both cases, the centers disappear at the same temperature and are restored after γ irradiation. Center II appears to correlate with the 250 °C TL peak and has the possibility to be associated with the high temperature 310 °C TL peak, due to their broad decay.

Acknowledgments

The authors wish to thank Ms. E. Somessari and Mr. C. Gaia, Instituto de Pesquisas Energeticas e Nucleares (IPEN), Brazil, for kindly carrying out the irradiation of the samples. This work was carried out with financial support from Fundação de Amparo à Pesquisa do Estado de São Paulo - FAPESP (Process number 2014/03085-0).

References

[1] S. Watanabe, N.F. Cano, L.S. Carmo, R.F. Barbosa, J.F.D. Chubaci, High- and very-high-dose dosimetry using silicate minerals, Radiat. Meas. 72 (2015) 66–69.
[2] S. Watanabe, N.F. Cano, T.K. Gundu Rao, L.M. Oliveira, L.S. Carmo, J.F.D. Chubaci, Radiation dosimetry using decreasing TL intensity in a few variety of silicate crystals, Appl. Radiat. Isot. 105 (2015) 119–122.
[3] R.F. Barbosa, N.F. Cano, S. Watanabe, R.A.S. Guttler, F. Reichmann, Thermoluminescence in two varieties of jadeite: irradiation effects and application to high dose dosimetry, Radiat. Meas. 71 (2014) 36–38.
[4] N.F. Cano, S. Watanabe, A.R. Blak, J.M. Yauri, Radiation effects on TL and EPR of sodalite and application to dosimetry, J. Phys. Conf. Ser. 249 (2010) 012022.
[5] N.F. Cano, J.M. Yauri, S. Watanabe, J.C.R. Mittani, A.R. Blak, Thermoluminescence of natural and synthetic diopside, J. Lumin. 128 (2008) 1185–1190.
[6] M.I. Teixeira, L.V.E. Caldas, Dosimetric characteristics of jasper samples for high dose dosimetry, Appl. Radiat. Isot. 70 (2012) 1417–1419.
[7] M.I. Texeira, A.P. Melo, G.M. Ferraz, L.V.E. Caldas, Application of jade samples for high-dose dosimetry using the EPR technique, Appl. Radiat. Isot. 68 (2010) 582–585.
[8] W.A. Deer, R.A. Howie, J. Zussman, An Introduction to the Rock-forming Minerals, 2nd ed., Longman, England, 1992.
[9] D.J. Henry, M. Novák, F.C. Hawthorne, A. Ertl, B.L. Dutrow, P. Uher, F. Pezzotta, Nomenclature of the tourmaline-supergroup minerals, Am. Mineral. 96 (2011) 895–913.
[10] F. Bosi, Tourmaline crystal chemistry, Am. Mineral. 103 (2018) 298–306.
[11] M. Akizuki, T. Kuribayashi, T. Nagase, A. Kitakaze, Triclinic liddicoatite and elbaite in growth sectors of tourmaline from Madagastar, Am. Mineral. 86 (2001) 364–369.
[12] A. Shtukenberg, I. Rozhdestvenskaya, O. Frank-Kamenetskaya, J. Bronzova, H. Euler, A. Kirfel, I. Bannova, A. Zolotarev, Symmetry and crystal structure of biaxial elbaite-liddicoatite tourmaline from the Transbaikalia region, Russia, Am. Mineral. 92 (2007) 675–686.
[13] J.M. Hughes, J. Rakovan, A. Ertl, G.R. Rossman, I. Baksheev, H.J. Bernhardt, Dissymmetrization in tourmaline: the atomic arrangement of sectorally zoned triclinic Ni-bearing dravite, Can. Mineral. 49 (2011) 29–40.
[14] S. Fortier, G. Donnay, Schorl refinement showing composition dependence of the tourmaline structure, Can. Mineral. 13 (1975) 173–177.
[15] D.J. MacDonald, F.C. Hawthorne, Cu-bearing tourmaline from Paraiba, Brazil, Acta Crystallogr. C 51 (1995) 555–557.
[16] F.C. Hawthorne, D. Henry, Classification of the minerals of the tourmaline group, Eur. J. Mineral. 11 (1999) 201–215.
[17] J.M. Hughes, A. Ertl, M.D. Dyar, E.S. Grew, M. Wiedenbeck, F. Brandstätter, Structural and chemical response to varying 4B content in zoned Febearing olenite from Koralpe, Austria, Am. Mineral. 49 (2004) 447–454.
[18] A. Abduriyim, H. Kitawaki, M. Furuya, D. Schwarz, Paraíba-type copper-bearing tourmaline from Brazil, Nigeria, and Mozambique: chemical fingerprinting by LA-ICP-MS, Gems Gemol. 42 (2006) 4–21.
[19] H. Beurlen, O.J.M. Moura, D.R. Soares, M.R.R. Silva, D. Rhede, Geochemical and geological controls on the genesis of gem-quality "Paraíba tourmaline" in granitic pegmatites from northeastern Brazil, Can. Mineral. 49 (2011) 277–300.
[20] P.G. Manning, An optical absorption study of the origin of colour and pleochroism in pink and brown tourmalines, Can. Mineral. 9 (1968) 678–690.
[21] P.G. Manning, Optical absorption spectra of chromium-bearing tourmaline, black tourmaline and buergerite, Can. Mineral. 10 (1969) 57–70.
[22] P.G. Manning, Effect of second–nearest–neighbour interaction on Mn^{3+} absorption in pink and black tourmalines, Can. Mineral. 11 (1973) 971–977.
[23] G.H. Faye, P.G. Manning, J.R. Gosselin, R.J. Tremblay, The optical absorption spectra of tourmaline: importance of charge-transfer processes, Can. Mineral. 12 (1974) 370–380.
[24] R.A. Ayuso, C.E. Brown, Manganese-rich red tourmaline from the Fowler talc belt, New York, Can. Mineral. 22 (1984) 327–331.
[25] V.T. Kazachenko, L.A. Butsik, V.I. Sapin, I.V. Kitaev, N.N. Barinov, G.A. Narnov, Vanadian-chromian tourmaline and vanadian muscovite in contact-metamorphosed carbonaceous rocks, Primorye, Russia, Can. Mineral. 31 (1993) 347–356.
[26] A. Ertl, J.M. Hughes, F. Pertlik, F.F. Foit, S.E. Wright, F. Brandstätter, B. Marler, Polyhedron distortions in tourmaline, Can. Mineral. 40 (2002) 153–162.
[27] F.C. Hawthorne, Bond-valence constraints on the chemical composition of tourmaline, Can. Mineral. 40 (2002) 789–797.
[28] I.A. Baksheev, O.E. Kudryavtseva, Nickeloan tourmaline from the Berezovskoe gold deposit, Middle Urals, Russia, Can. Mineral. 42 (2004) 1065–1078.
[29] F. Bosi, Disordering of Fe^{2+} over octahedrally coordinated sites of tourmaline, Am. Mineral. 93 (2008) 1647–1653.
[30] M. Kutzschbach, B. Wunder, D. Rhede, M. Koch-Müller, A. Ertl, G. Giester, W. Heinrich, G. Franz, Tetrahedral boron in natural and synthetic HP/UHP tourmaline: evidence from Raman spectroscopy, EMPA, and single-crystal XRD, Am. Mineral. 101 (2016) 93–104.
[31] A. Watenphul, M. Burgdorf, J. Schlüter, I. Horn, T. Malcherek, B. Mihailova, Exploring the potential of Raman spectroscopy for crystallochemical analyses of complex hydrous silicates: II. Tourmalines, Am. Mineral. 101 (2016) 970–985.
[32] A. Ertl, U. Kolitsch, M.D. Dyar, J.M. Hughes, G.R. Rossman, A. Pieczka, D.J. Henry, F. Pezzotta, S. Prowatke, C.L. Lengauer, W. Körner, F. Brandstätter, C.A. Francis, M. Prem, E. Tillmanns, Limitations of Fe^{2+} and Mn^{2+} site occupancy in tourmaline: evidence from Fe^{2+}- and Mn^{2+}-rich tourmaline, Am. Mineral. 97 (2012) 1402–1416.
[33] O.S. Vereshchagin, I.V. Rozhdestvenskaya, O.V. Frank-Kamenetskaya, A.A. Zolotarev, Ion substitutions and structural adjustment in Cr-bearing tourmalines, Eur. J. Mineral. 26 (2014) 309–321.
[34] A. Ertl, O.S. Vereshchagin, G. Giester, E. Tillmanns, H.P. Meyer, T. Ludwig, I.V. Rozhdestvenskaya, O.V. Frank-Kamenetskaya, Structural and chemical investigation of a zoned synthetic Cu-rich tourmaline, Can. Mineral. 53 (2015) 209–220.
[35] C. Castañeda, S.G. Eeckhout, G.M. Costa, N.F. Botelho, E. Grave, Effect of heat treatment on tourmaline from Brazil, Phys. Chem. Miner. 33 (2006) 207–216.
[36] P.G. Manning, Effects of second nearest neighbors interacting on Mn^{3+} absorption in tourmalines, Can. Mineral. 9 (1973) 723–730.
[37] A. Maneewong, K. Pangza, N. Jangsawang, T. Charoennam, Effect of heat treatment and electron beam irradiation tourmaline: UV–visible, EPR, and mid-IR spectroscopic analyses, J. Sci. Technol. 13 (2016) 993–1003.
[38] K. Krambrock, M.V.B. Pinheiro, K.J. Guedes, S.M. Medeiros, S. Schweizer, J.M. Spaeth, Correlation of irradiation-induced yellow color with the O^- hole center in tourmaline, Phys. Chem. Miner. 31 (2004) 168–175.
[39] M.B. Camargo, S. Isotani, Optical absorption spectroscopy of natural and irradiated pink tourmaline, Am. Mineral. 73 (1988) 172–180.
[40] A. Maneewong, B.S. Seong, E. Shin, J.S. Kim, V. Kajornrith, Color change of tourmaline by heat treatment and electron beam irradiation: UV–visible, EPR, and Mid-IR spectroscopic analyses, J. Korean Phys. Soc. 68 (2016) 83–92.
[41] R.I. Mashkovtsev, S.Z. Smirnov, J.E. Shigley, The features of the Cu^{2+}-entry into the structure of tourmaline, J. Struct. Chem. 47 (2006) 252–257.
[42] J. Babinska, K. Dyrek, A. Pieczka, Z. Sojka, X and Q band EPR studies of paramagnetic centres in natural and heated tourmaline, Eur. J. Mineral. 20 (2008) 233–240.
[43] M.J. Buerger, C.W. Burnham, D.R. Peacor, Assessment of the several structures proposed for tourmaline, Acta Cryst. 15 (1962) 583–590.
[44] G. Kitis, J.M. Gomez-Ros, J.W.N. Tuyn, Thermoluminescence glow curve *deconvolution* functions for first, second and general order kinetics, J. Phys. D: Appl. Phys. 31 (1998) 2636–2641.
[45] H.G. Balian, N.W. Eddy, Figure-of-Merit (FOM), an improved criterion over the normalized chi-squared test for assessing goodness-of-fit of gamma-ray spectral peaks, Nucl. Instrum. Methods 145 (1977) 389–395.
[46] P.W. Atkins, N. Keen, M.C.R. Symons, H.W. Wardale, Unstable intermediates. Part XX. Hydrogen atoms trapped in phosphates, J. Chem. Soc. 0 (1963) 5594–5598.
[47] S. Ogawa, R.W. Fessenden, Ring inversion in cyclohexyl radical, J. Chem. Phys. 41 (1964) 994–998.
[48] R. Livingston, A. Weinberger, Atomic and molecular hydrogen yields from irradiated acids, J. Chem. Phys. 33 (1960) 499.
[49] R. Livingston, H. Zeldes, E.H. Taylor, Paramagnetic resonance studies of atomic hydrogen produced by ionizing radiation, Discuss. Faraday Soc. 19 (1955) 166.
[50] J.C. Vedrine, B. Imelik, E.G. Derouane, Influence of the physical state of three different aluminum hydroxides on the interaction between trapped h atom and lattice protons: an EPR and ENDOR study, J. Magn. Res. 16 (1974) 95–109.
[51] E.G. Derouane, J.C. Vedrine, Characterization of γ-ray induced paramagnetic centers in bayerite by means of EPR and ENDOR spectroscopies, J. Chem. Phys. 65 (1976) 927.
[52] L.O. Andersson, The positions of H^+, Li^+ and Na^+ impurities in beryl, Phys. Chem. Miner. 33 (2006) 403–416.
[53] R.G. Burns, Mineralogical Applications of Crystal Field Theory, 2nd ed., Cambridge University Press, Cambridge, UK, 1993.